Available online at www.sciencedirect.com
SCIENCE DIRECT
Cement and Concrete Research 36 (2006) 1389–1398
Cement and Concrete Research

Stability of ancient masonry towers: Stress redistribution due to drying, carbonation, and creep

Daniele Ferretti [a], Zdeněk P. Bažant [b,*]

[a] University of Parma, Parco Area delle Scienze 181/A, 43100 Parma, Italy
[b] Northwestern University, 2145 Sheridan Road, CEE, Evanston, Illinois 60208, USA

Received 23 December 2004; accepted 16 March 2006

Abstract

Extending the analysis of the evolution of pore humidity and carbonation presented in a preceding paper by Ferretti and Baz˘ant, this paper analyzes the redistribution in time of vertical normal stresses across the multiple-leaf wall of ancient towers, using the example of collapsed Pavia Tower. It is shown that stress redistribution due to nonuniform shrinkage and nonuniform creep across the wall, including the additional redistribution due to cracking, produces in the masonry cladding of the wall very large compressive stresses that reach, after centuries, the level of compression strength of the cladding.

Keywords: Creep; Humidity; Diffusion; Long-term performance; Tower

1. Introduction

This study is motivated by the sudden collapse of the Civic Tower of Pavia in 1991, at the age of about eight centuries, without any warning signal. The possible causes of failure were examined in [1–3] considering the evidence from collapse, tests on the ruins and finite element analysis. Researchers concluded that creep damage, triggered by stress concentrations, was the main cause of failure [3]. Other possible concomitant causes were pointed out, such as temperature fluctuations, vibrations produced by bells, soil vibrations, and action of wind.

Aside from these phenomena, we propose redistribution of stresses in time as a major cause of failure. The redistribution is caused by nonuniformity of carbonation, drying shrinkage and drying creep, and is modified by distributed cracking. These phenomena arise from the slow evolution of pore humidity in time.

The preceding part of this study [4] addressed the evolution of pore humidity and carbonation degree across the wall of the tower. Based on this background information, the present paper will analyze the redistribution of vertical normal stresses due to self-weight across the wall. No mathematical model seems available for this ancient material. Therefore, we will adapt an existing model proposed for Portland cement concrete. This analogy seems possible because the underlying physical considerations are similar for both materials. Although the results will be only approximate, they will serve to quantify the phenomena involved, which in the past were studied only qualitatively. Moreover, the results of this stress analysis are needed for a subsequent study that will address the fracture process with size effect.

2. Humidity diffusion and carbonation

The Civic Tower of Pavia, like many other medieval towers, had massive multiple leaf walls. Observing the wall section cut out by Calvi [5] from a block that survived the collapse (Fig. 1), we can see the external regular brickwork which served during construction as a mould for casting the core. The core is a conglomerate, built layer by layer from stones and brick pebbles embedded in mortar and alternated with thick courses of limebased mortar [3]. The maximum aggregate size in the mortar ranged between 20 and 60 mm [6]. The conglomerate differs from regular masonry as well as Portland cement concrete and is called the ‘ancient concrete’ [1,3].

* Corresponding author.
E-mail addresses: daniele.ferretti@unipr.it (D. Ferretti), z-bazant@northwestern.edu (Z.P. Bažant).

0008-8846/$ - see front matter © 2006 Elsevier Ltd. All rights reserved.
doi:10.1016/j.cemconres.2006.03.014

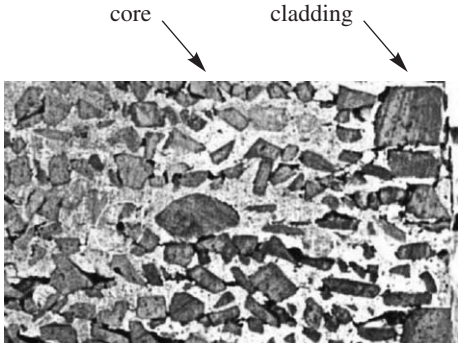

Fig. 1. A section of a wall of the Civic Tower of Pavia cut from a block that survived collapse (after [5]).

Since little research dealt with this material, previous studies treated it as a poor Portland cement concrete and assumed it to be homogeneous and isotropic [1,6]. In contrast to concrete, cementation depends on the reaction of hydrated lime with atmospheric carbon dioxide (CO_2), which produces a durable carbonate matrix [7]. The process is controlled by humidity diffusion through ancient concrete, which causes a reduction of pore water content and allows diffusion of CO_2 from the outside to the pores. The reaction of hydrated lime with CO_2 then produces calcium carbonate and water. By reducing total porosity, carbonation retards diffusion of humidity. So, carbonation, humidity diffusion, and CO_2 diffusion interact. To model these phenomena and their interaction, three coupled diffusion–reaction equations must be solved. Such a model has been formulated and used in [4,8–10]. Here we describe the model and use it for spatially one-dimensional calculations.

The first partial differential equation governs the rate of relative concentration of carbonate, $\mathcal{R} = [CaCO_3]/[CaCO_3]_{max}$

$$\frac{\partial \mathcal{R}}{\partial t} = \alpha_1 f_1(h) f_2(c) f_3(\mathcal{R}) f_4(T) \tag{1}$$

where h=relative pore humidity, c=[CO_2], T=absolute temperature, and t=time (age of wall). Coefficient $f_1(h)$ expresses the effect of relative humidity h. Coefficients $f_2(c)$ and $f_3(\mathcal{R})$ describe the influence of concentration of carbon dioxide, c, and of the degree of carbonation, $\mathcal{R}$.

The second partial differential equation governs moisture diffusion in terms of relative humidity h in the pores;

$$\frac{\partial h}{\partial t} = \frac{\partial}{\partial x}\left(C\frac{\partial h}{\partial x}\right) + \frac{\partial h_s}{\partial t} + \alpha_2 \frac{\partial \mathcal{R}}{\partial t} \tag{2}$$

where C=diffusivity of h, h_s=self-desiccation humidity (humidity variation caused by water consumed in chemical reactions), and α_2=coefficient that governs the effect of water liberated during carbonation.

The third partial differential equation describes the diffusion of carbon dioxide

$$\frac{\partial c}{\partial t} = \frac{\partial}{\partial x}\left(D_c\frac{\partial c}{\partial x}\right) - \alpha_3 \frac{\partial \mathcal{R}}{\partial t} \tag{3}$$

where D_c=diffusivity of CO_2, and α_3=coefficient governing the sink term due to the consumption of CO_2 by carbonation. For more details see [4].

The system of partial differential Eqs. (1), (2), and (3) is solved by finite element method in the sense of Galerkin. In the domain $x \in (0, D)$, a uniform mesh of one-dimensional elements is introduced. The elements are based on Lagrangian quadratic shape functions. The solution in space and time is obtained following the procedure described in [4]. At any time t, the solution provides the profiles of $\mathcal{R}$, h, and c across thickness D of the wall. The variation of h in time produces creep and shrinkage in lime mortar. At the same time, its mechanical properties vary with carbonation $\mathcal{R}$, which substantially depends on humidity h.

3. Interaction of humidity diffusion, creep, and fracture

Only few studies are available for creep and shrinkage of lime mortar concrete [3,11,12]. They all indicate that a mathematical treatment similar to low strength Portland cement concrete is possible. Some investigators nevertheless expressed the opinion that some differences in treatment were necessary. In the case of lime concrete, there is no cement gel, and no hydration but only carbonation, unless the mortar contains pozzolanic materials (such as pozzolana or brick pebbles, and dust), with which the hydrated lime reacts [13]. In that case a certain amount of cement gel and calcium silicates is present and the chemical similarity is stronger.

Consequently, at the present level of knowledge, it appears logical to adopt a creep and shrinkage model that has been physically justified for Portland cement concrete. For the reasons described in [14], model B3 [15] is adopted here, but with the hydration features removed.

3.1. Mechanisms of creep and aging

At service stresses, which are less than about one half of the strength, and in the absence of cracking, the creep strain depends on stress linearly and may, therefore, be characterized by the compliance function, $J(t, t')$, defined as the strain at time t caused by a unit uniaxial stress applied at time t'. According to model B3 [15]:

$$\dot{J}(t,t') = v^{-1}(t)\dot{C}_g(\theta) + 1/\eta_f \tag{4}$$

$$v^{-1}(t) = (\lambda_0/t)^m + q_3/q_2 \tag{5}$$

$$\dot{C}_g(\theta) = q_2 \frac{n\theta^{n-1}}{\lambda_0^n + \theta^n} \tag{6}$$

where $\dot{J}(t, t')$=d$J(t, t')$/dt=compliance rate. The initial value $J(t', t')$=q_1=age-independent constant; θ=$t-t'$=load duration; λ_0=1 day; m=0.5; $n \approx 0.1$–0.2; q_2, q_3=material parameters; $C_g(\theta)$=compliance function for a non-ageing constituent; η_f=effective viscosity for viscous flow; and $v(t)$=volume of cement gel or carbonate per unit volume of material, growing due to hydration or carbonation. According to the solidification theory, aging is described by the volume growth $v(t)$ of cement gel or carbonates into the pores. In Portland cement concrete, the volume growth of hydration products is relatively short-lived, terminating in about one

year, if sufficient water is supplied. In lime concrete the volume growth of carbonated products is fast once carbonation occurs, although this may take a very long time due to diffusion. To explain and model the long-term aging in creep and the effect of pore humidity variation, a flow term is introduced. For creep of sealed specimens at constant temperature, called the basic creep, the flow term may be written as $1/\eta_f = q_4/t$ where q_4 is a material parameter. When the specific water content (mass of water per unit volume of concrete) varies because of moisture diffusion, hydration and carbonation, the flow term is modified by introducing the concept of microprestress [16,17].

3.2. Microprestress and coupling of creep with humidity changes

In Portland cement concrete, microprestress is regarded as a measure of the stress peaks at creep sites in the nanostructure of cement gel [16]. The microprestress is considered to be unaffected by the applied load and to be produced solely by chemical volume changes and by drying or wetting. Expressed in terms of microprestress S, the flow term becomes [16,17]

$$1/\eta_f = q_4'(p-1)S^{p-2}\dot{S} \tag{7}$$

where q_4' = coefficient that depends on the type of concrete, and $p \approx 2$. The microprestress relaxes in time and its evolution at each point of a concrete structure, at constant temperature and variable humidity h, may be solved from the differential equation

$$\dot{S} + c_0 S^p = -c_1 |\dot{h}/h| \tag{8}$$

where c_0, c_1 = positive constants. The absolute value is introduced to reflect the experimental observation that not only drying but also wetting accelerates creep.

The main justification of the concept of microprestress relaxation is that it describes not only drying creep but also the long-term aging of creep, manifested by a decrease of flow viscosity. The concept of microprestress seems reasonable also for lime concrete since lime was observed to undergo aging, especially for alternating humidity [18]. Of course, the physical justification given in [18] differs from the case of concrete, and the model coefficients need to be recalibrated by tests.

At variable environmental conditions, time t in Eq. (5) must be replaced by the equivalent hydration time

$$t_e = \int_0^t \beta_h \beta_T \mathrm{d}t \tag{9}$$

where $\beta_T = \exp(Q_h/RT_0 - Q_h/RT)$, $T_0 = 296\,\mathrm{K}$, $Q_h/R \approx 2700\,\mathrm{K}$, and, in analogy to concrete, $\beta_h = [1+(5-5h)^4]^{-1}$. The loading duration $\theta = t - t'$ in Eq. (6) must be replaced by $\theta = t_r - t_r'$, where

$$t_r = \int_0^t \psi_h \psi_T \mathrm{d}t \tag{10}$$

is the reduced time for creep, different from t_e; $\psi_h = 0.1 + 0.9h^2$, $\psi_T = \exp(Q_v/RT_0 - Q_v/RT)$, and $Q_v/R \approx 5000\,\mathrm{K}$. To take into account carbonation, the equivalent hydration time t_e could be modified by introducing in Eq. (9) an additional factor $\beta_{\mathcal{R}}$, but no data exist in this regard.

3.3. Free shrinkage

Because of nonuniform distribution of pore humidity h, the free (unrestrained) shrinkage strain rates $\dot{\epsilon}_{sh}$ at various points of the structure are in general different, and their incompatibility causes microcracking or cracking. For this reason, $\dot{\epsilon}_{sh}$ cannot be measured directly and must be determined indirectly by finite element analysis of the overall shrinkage of specimens [15,19–21]. Data fitting by inverse analysis [16] confirms that

$$\dot{\epsilon}_{sh} = k_{sh}\dot{h} \tag{11}$$

where k_{sh} = constant coefficient. Only few measurements of shrinkage of lime mortar are reported in the literature [11,12,22]. No useful data seems available regarding drying creep (or Pickett effect) and the separation of the effects of cracking and stress-induced shrinkage in the sense of [20]. Thus, the simple behavior expressed by Eq. (11) must be co-opted.

At early ages of ancient concrete, the excess of water is lost and shrinkage occurs. During this process, diffusion of CO_2 from the environment into partially dried pores activates the carbonation process of portlandite into calcite [23], and thus carbonation shrinkage takes places (carbonation shrinkage of the compacts of hydrated lime was observed in [24]). In lime mortar specimens, sand grains must resist and reduce carbonation shrinkage, although some authors, e.g. [7], were unable to detect it. This point is still debatable and further research is needed. For this reason, we neglect carbonation shrinkage.

3.4. Cracking and fracture mechanics aspects

Tensile stress produced by hindered shrinkage usually causes microcracking or cracking [19,25]. For deep drying penetration of massive structures, cracking may localize into widely spaced large macro-cracks, surrounded by shorter, tiny, and closely spaced cracks. In this situation, the structural and diffusion problems may be coupled because cracks wider than 0.5 mm influence diffusivity. In towers, due to self-weight, horizontal cracking is partially suppressed, and so a network of closely spaced narrow cracks is likely. Thus, the diffusion problem may be assumed to be uncoupled to cracking and can be solved separately, before the stress analysis.

To take the fracture mechanics aspects of cracking into account in a simple manner, the crack band model is used [26], and cracking is assumed to localize into discrete cracks with a certain characteristic spacing s. Because parallel adjacent crack bands cannot overlap, the minimum possible spacing of such cracks must be taken equal to the empirically known width w_c of the crack band (or the fracture process zone), which must be considered as a material property. For cement concrete, roughly $w_c \approx 2d_a$ to $3d_a$ where d_a is the maximum aggregate size. For ancient concrete, if cracking occurs in the lime mortar, we use the same estimate but d_a is the maximum aggregate size of the mortar. For masonry, since cracking occurs in the joints, we hypothesize w_c to be equal to the height of the bricks.

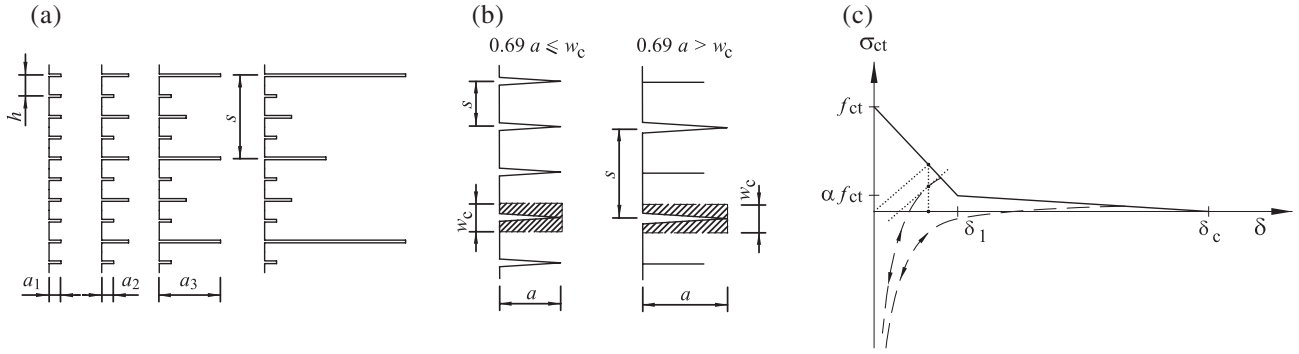

Fig. 2. Cracking: (a) evolution of a system of parallel shrinkage cracks and crack spacing as a function of crack length (after [29]); (b) crack system limited by minimum spacing w_c equal to width of crack band (fracture process zone); (c) tensile stress–strain relation of cracked concrete based on the cohesive crack model [30].

When the parallel cracks get too long compared to their spacing, every other crack closes and the spacing of the remaining (dominant) cracks doubles. Based on the analysis of equilibrium path bifurcation in a system of parallel thermal cracks [27,28], it was shown in [29] that the spacing of the dominant (open) cracks increases on the average as $s=0.69a$ where a is the length of the cracks (Fig. 2a). For the aforementioned reasons, the general rule for the dominant crack spacing may be written as

$$s = \max(w_c, 0.69a). \tag{12}$$

According to the crack band model, the accumulated cracking strain may be defined as $\epsilon_{cr}=\delta/s$ where δ is the opening width of the actual cracks. The stress corresponding to ϵ_{cr} is obtained from the bilinear softening function (Fig. 2c) of the cohesive crack model proposed in [30], which is written in secant form:

$$\sigma(\epsilon_{cr}) = \sigma(\delta/s) = E_{cr}\epsilon_{cr}. \tag{13}$$

Differentiating in time, we get the stress rate

$$\dot{\sigma} = E_{cr}\dot{\epsilon}_{cr} + \dot{E}_{cr}\epsilon_{cr} \tag{14}$$

whereas the corresponding incremental strain is

$$\dot{\epsilon}_{cr} = \frac{1}{E_{cr}}\dot{\sigma} - \frac{\dot{E}_{cr}}{E_{cr}}\epsilon_{cr} = C_{cr}\dot{\sigma} + \dot{\epsilon}''_{cr}. \tag{15}$$

During shrinkage (and raising of the tower), some zones undergo unloading or unloading–reloading cycles, in which case Eq. (14) is replaced by $\dot{\sigma}=E_{cr}\dot{\epsilon}_{cr}$. At a given ϵ_{cr}, the slope of the unloading curve represents the corresponding secant stiffness of the virgin curve (Fig. 2c). For the sake of simplicity, reloading is assumed to follow the same curve as unloading, even though a hysteretic behavior could be introduced [19]. Unloading and reloading are complicated by the fact that during time the flow of water into the cracks may produce re-crystallization of the calcium carbonate and the cracks can thus be sealed. This effect is neglected and so is viscosity of the fracturing process (e.g. [31]).

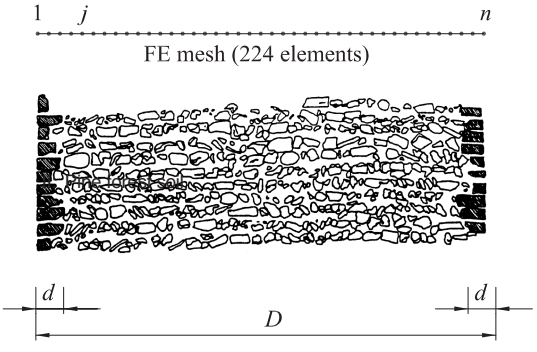

Fig. 3. Cross section of a wall of the tower: finite element mesh for diffusion and stress analyses in one dimension.

4. The case of Pavia Tower: calibration of main parameters

The numerical procedure used to solve the creep and shrinkage problem is described in the Appendix. It was applied to study the wall at the base of Pavia Tower. Its wall (Fig. 3) has indefinite height and width, whereas the total base is $D=2.8$ m. At both edges it is lined by a good coursed masonry cladding of thickness $d=0.15$ m.

4.1. Material properties

Measurements in [5] on small size panels (approximately $700\times500\times300$ mm) recovered from the ruins of the tower provide the following data. For the core: aggregate size

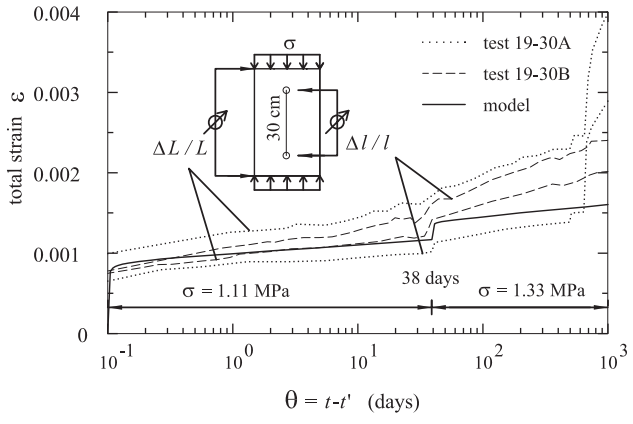

Fig. 4. Calibration of B3 model by means of creep strains measured in [6] on the ruins of Pavia Tower.

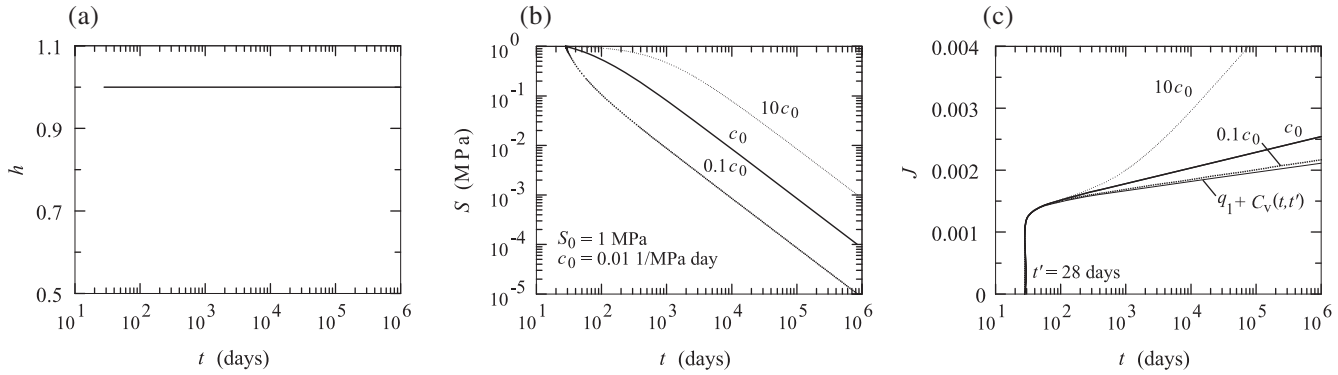

Fig. 5. Calibration of coefficient c_0 of microprestress at constant relative pore humidity: (a) relative pore humidity h; (b) microprestress S; (c) strain J.

$d_a=20\,\text{mm}$, secant Young's modulus $E_c=2670\,\text{MPa}$, Poisson ratio $\nu=0.14$, compressive strength $f'_c=3.1\,\text{MPa}$, tensile strength $f_{ct}=f'_c/20$, $w_1=0.2\,\text{mm}$, $w_c=0.8\,\text{mm}$, and specific weight $\gamma_c=18.1\,\text{kN/m}^3$. For the masonry cladding: secant Young's modulus $E_m=2650\,\text{MPa}$, Poisson ratio $\nu_m=0.16$, compressive strength $f'_m=4.1\,\text{MPa}$, tensile strength $f_{mt}=f'_m/20$, and specific weight $\gamma_m=17.2\,\text{kN/m}^3$. The bricks have the average height of 60 mm, and the mortar joints 20 mm. Perfect bond between masonry cladding and lime concrete core is assumed, as suggested by tests on blocks composed of both materials [6]. The mechanical properties were measured on carbonated blocks that survived the collapse. As pointed out in [23], the scarce literature about these materials and the controversial results do not explain how to consider the variation of mechanical properties with the degree of carbonation $\mathcal{R}$, and so the properties are considered constant.

4.2. Creep

The creep model is calibrated by long-term tests in [6] and [3] on specimens recovered from the ruins, and the early-age behavior is co-opted from concrete. In these tests, specimens labeled 19-30A and 19-30B were subjected to an initial constant stress $\sigma=1.11\,\text{MPa}\approx 0.4f'_c$. After 30 days, the stress was increased to $\sigma=1.38\,\text{MPa}$. For the first period of the test (1000 days) the strain history, measured on the bases of L=specimen height and $l=300\,\text{mm}$, is represented in Fig. 4. The means of the scattered curves are used here to calibrate the creep model; exponent $n=0.15$ in Eq. (4) is chosen to enhance long-term creep; parameters $q_1=0.0005\,\text{MPa}^{-1}$, $q_2=0.0025\,\text{MPa}^{-1}$, $q_3=0.2q_2$, $m=0.5$ provide the numerical curve represented in Fig. 4 by a thick line. Only a few tests are available for creep and drying creep of masonry brickwork [12,32], and so the aforementioned parameters are also used for the mortar joints in the cladding. In compatibility equations (31), the overall creep strains of the cladding are reduced by the ratio of the thickness of joint to the thickness of brick and joint, which is about 1/4.

4.3. Microprestress

The parameters for microprestress in Eq. (8) are calibrated to obtain the flow term. The initial value of microprestress at $t=28\,\text{days}$ is considered to be $S_0=1\,\text{MPa}$. Like the compressive strength, this is one order of magnitude lower than a typical value for normal Portland cement concrete. At constant humidity $h=1$ (Fig. 5a), the evolution in time of microprestress is governed by parameter c_0, taken as $0.01\,\text{MPa}^{-1}\ \text{day}^{-1}$. Although microprestress decays greatly over the centuries (Fig. 5b), over a long time period, it nevertheless suffices to produce an important flow contribution to the compliance $\hat{J}$, characterized by $q'_4=5\times10^{-7}$ (Fig. 5c). If c_0 were replaced by $0.1c_0$, the microprestress would decay so fast (Fig. 5b) that the flow contribution to the compliance $\hat{J}$ would become negligible for

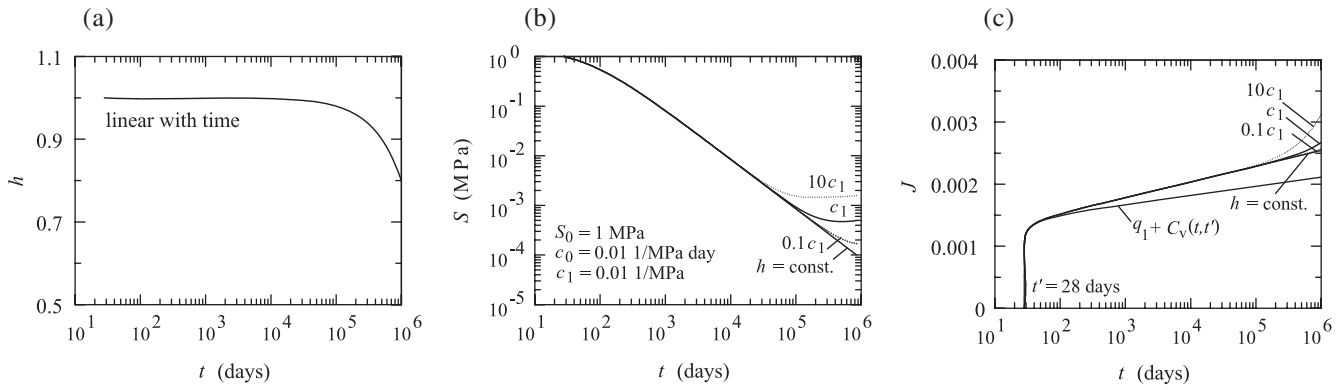

Fig. 6. Calibration of coefficient c_1 of microprestress at variable relative pore humidity: (a) relative pore humidity h; (b) microprestress S; (c) strain J.

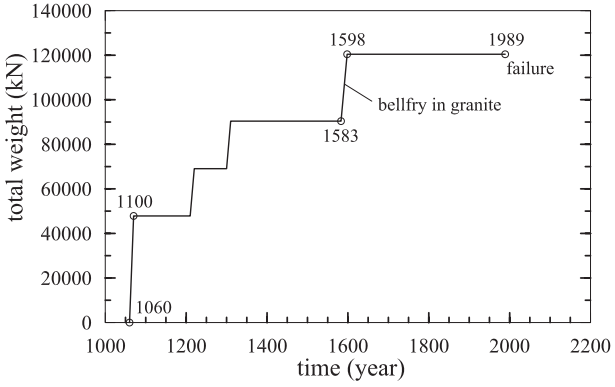

Fig. 7. Total load ramp $N_z(t)$.

long times (centuries) (Fig. 5b). If replaced by $10c_0$, an implausibly large microprestress would arise (Fig. 5b), and the flow strain would probably be overestimated (Fig. 5c).

The effect of pore humidity h on microprestress is controlled by coefficient c_1, taken as $0.01\,\mathrm{MPa}^{-1}$. A linear reduction of humidity with time (Fig. 6a) produces higher values of microprestress (Fig. 6b) and increases the flow contribution to $\hat{J}$, especially after centuries (Fig. 6c). The value $0.1c_1$ would give only a modest effect of humidity (Fig. 6b), whereas $10c_1$ would give an excessive effect compared to standard behavior of concrete.

4.4. Shrinkage

Coefficient $k_{sh}=0.003$ in Eq. (11) is assumed for lime mortar concrete. The same applies for masonry joints, although their shrinkage and cracking are largely affected in the construction stage, during which water moves between the mortar joints and bricks [33].

4.5. Load history

Based on ancient manuscripts on similar towers, the average speed of construction is assumed to be about $5\,\mathrm{m\ year}^{-1}$. Because the tower was probably built in four stages, described in [2], an extended time ramp of loading by self-weight $N_z(t)$ is assumed (Fig. 7). The self-weight is considered to be the only permanent load to be taken into account for creep analysis. Note in Fig. 7 that a belfry consisting of heavy granite blocks was built in 1583, and this increased the weight of the tower by 30%. Additional stresses due to wind can be quite important for ancient towers but are not of long enough durations for affecting creep. Seismic effects are neglected for the same reason, and thermal cycles probably affect only a relative thin surface layer of the wall, but further studies are needed.

5. Results of analysis of Pavia Tower

The problem of diffusion and carbonation is solved separately in advance, as described in a preceding paper [4]. In particular, at the surfaces of the wall, which are in contact with the environment, convective boundary conditions $\partial h/\partial x=\beta(h-h_e)$ are assumed; $\beta=5\,\mathrm{mm\ day}^{-1}$ (surface convection coefficient), and $h_e=0.8+0.07\cos(2\pi t)$ (environmental relative humidity). The essential boundary conditions are $c(0,t)=c(D,t)=0.035\%$ and $\mathcal{R}(0,t)=\mathcal{R}(D,t)=1$. The initial conditions at

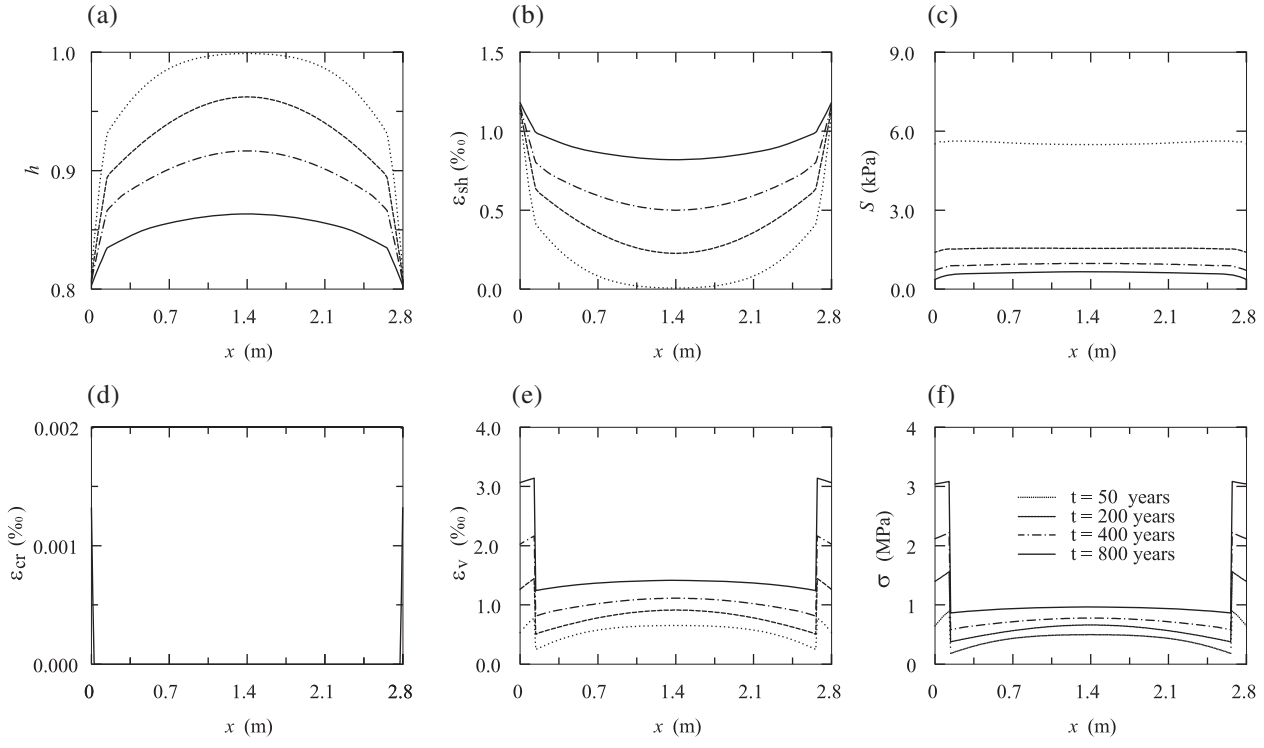

Fig. 8. Profiles after $t=50$, 200, 400, 800 years: (a) relative pore humidity h; (b) shrinkage strain ϵ_{sh}; (c) microprestress S; (d) cracking strain ϵsubcr; (e) viscous strain ϵ_v; (f) stress σ.

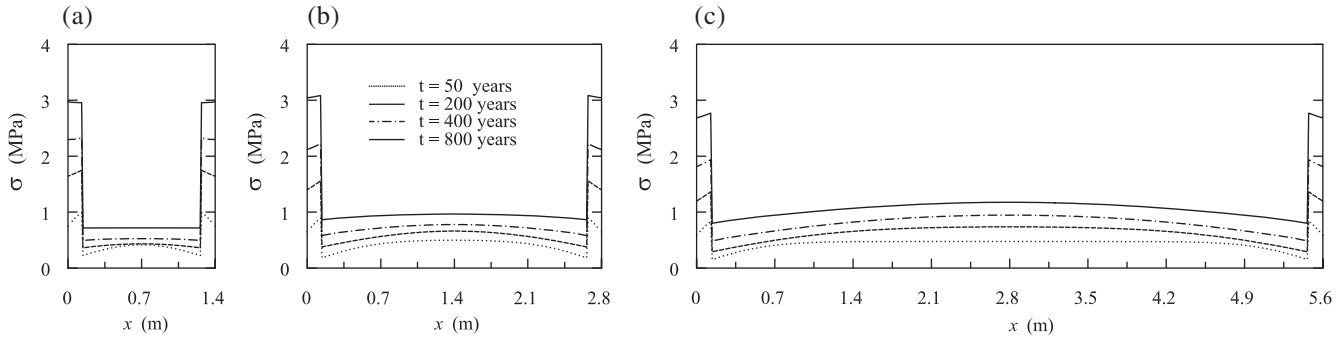

Fig. 9. Evolution of stress profiles in walls of different thickness: (a) $D=1.4$ m; (b) $D=2.8$ m; (c) $D=5.6$ m.

time $t=t_0$ are $h(x, t_0)=1.0$, $c(x, t_0)=0$, and $\mathcal{R}(x, t_0) = 0$ for all $x\in]0, D[$. All the materials parameters and coefficients are reported in [4], which also gives the detailed results of finite element analysis. Fig. 8a shows pore relative humidity profiles at the ages of 50, 200, 400, and 800 years. Their slow evolution controls the temporal scale of shrinkage strains ϵ_{sh} and microprestresses S, which are plotted in Fig. 8b,c. Fig. 8e,f shows the corresponding distribution of creep strains ϵ_v and vertical compressive stresses σ throughout the core and the mortar joints of the cladding at the base of the tower.

Initially, concrete shrinks near the cladding (Fig. 8b), producing tensile stresses which exhaust the tensile strength and cause a modest cracking near the cladding (Fig. 8d). To balance the tensile stresses, the compressive stresses increase slightly in the core of the wall.

There are several distinct sources of stress variations over centuries (Fig. 8f): (1) During construction stages, vertical compressive stresses increase because of increase of self-weight, causing crack closure. (2) After many centuries, the central portion of the wall shrinks significantly (Fig. 8b), and thus cracks tend to close (Fig. 8d). (3) The stress relaxation due to creep causes stresses nonuniformity to diminish with the passage of time (Fig. 8e). (4) Since the cladding creeps and shrinks only in the mortar joints (the creep of the bricks being negligible), the stresses and strains in the cladding must increase to maintain plane cross sections. For all these reasons, the vertical compression stress in the cladding roughly reaches, after many centuries, the strength measured in laboratory tests [1,2]. This can explain vertical splitting microcracks observed in the cladding of Pavia Tower 20 years before failure [2], and also in many other towers.

For comparison, the analysis was repeated to study the stress evolution in the walls of different thickness, $D=1.4$, 2.8, 5.6 m. See Fig. 9, which shows the dependence of the shape of the stress profiles on the wall thickness (due to moisture diffusion) and the consequent size dependence of shrinkage and creep [4]. This is one reason for the size effect on nominal compressive strength of the wall.

6. Conclusions and closing comments

Stress redistribution across the wall of the Pavia Tower, engendered by drying and creep, leads to a gradual increase of compression stresses in the masonry cladding. Computations, taking into account distributed cracking in the lime mortar core, indicate that after about eight centuries these stresses reach the approximate level of compression strength of the masonry. This is likely a major cause for the collapse of Pavia Tower, although many phenomena may also contribute. However, comparison of the stresses with the strength in a structure of the size of the tower does not suffice to assess the danger of collapse because the material is brittle. Fracture mechanics must be used and the consequent size effect taken into account. This will be the subject of a following study.

Some researchers noted that, because the ratio of the cladding thickness to the total thickness of the wall is very small (around 1/10 to 1/20), the cladding was not contributing much to the strength of the wall [1]. Indeed, if the stresses were uniform, the core of the tower would be able to carry the vertical load without cladding. However, because the stress is nonuniform and because a localized failure acts as a notch, causing stress concentration, the failure of the cladding must cause the stress to become critical elsewhere (near the mortar next the cladding), and thus the failure can propagate even if the average stress does not exceed the strength limit.

Seemingly, different opinions of various researchers [3,34] can be reconciled with the present model. For example, nonlinear creep has been suggested as responsible for damage propagation [3], but since damage evolution and localization are time- and rate-dependent they are essentially equivalent to nonlinear creep. Others [34] suggested that increase of stress concentrations due to wind loading during storms can trigger rapid nonlinear creep [34], sometimes called the secondary and tertiary creep, but mathematically this is equivalent to time dependent damage evolution (which eventually accelerates, like tertiary creep, due to decreasing undamaged cross section of material). In Pavia Tower, the zone particularly endangered by stress concentrations was the stairwell at the base, where the stairs passed through the wall along all the four sides of the tower, leaving on the sides two walls of thicknesses 1.4 and 0.6 m instead of one wall of thickness 2.8 m. Thus cladding failure near the stairwell is most dangerous. Also vibrations produced by bells, and temperature fluctuations, could produce fatigue and damage propagation. Because of scant data, a unique cause of failure is hard to identify.

So far, the diverse failure mechanisms were discussed mainly qualitatively and therefore their relevance is not sufficiently

understood. Introduction of mathematical models to describe them is indispensable to quantify their effects and decide their relevance in various situations.

Because sufficient experimental data are lacking at present, it is necessary to exploit analyses with Portland cement concrete which exhibits many similar characteristics. The analysis shows the stress redistribution due to nonuniform shrinkage and differential creep evolving over centuries can explain attainment of the strength limit within the wall, which can serve to trigger damage or fracture propagation. Once broader experimental basis becomes available, updating and recalibration of the model will be appropriate.

Acknowledgment

Partial financial support from the U.S. National Science Foundation under grant CMS-0301145 is gratefully acknowledged.

Appendix A. Details of numerical solution

To study the behavior of the wall depicted in Fig. 3, the diffusion and structural problems have to be solved in space and time. As they are assumed to be uncoupled, the diffusion problem is solved in advance of structural analysis. In particular, the time is divided into discrete times t_r ($r=1, 2,\ldots, N$) with uniform steps $\Delta t=t_{r+1}-t_r$. Nodes of coordinates x_i ($i=1, 2,\ldots, n$) subdivide the wall thickness D into one-dimensional finite elements (Fig. 3). Spacing $\Delta x=x_{i+1}-x_i$ is kept constant to capture the advancing front of carbonation. The problem of moisture diffusion, carbonation, and carbon dioxide diffusion is solved in space and time via the finite element method, following the procedure described in [4].

Once humidity profiles (given by the values of the pore relative humidity h at each node x_i) at each time step t_r are obtained, the microprestress is computed by numerical integration of Eq. (8) (in which the classical second order backward difference formula [35] is used);

$$S_{r+1}=\frac{4}{3}S_r-\frac{1}{3}S_{r-1}+\frac{2}{3}\Delta t\left(-c_0S_{r+1}^{p}-c_1\left|\frac{\Delta h/\Delta t}{h_{r+1}}\right|\right) \tag{16}$$

where Δh is the humidity increment over Δt. This formula, which is implicit, is also used to integrate the diffusion problem in time. Iterations are necessary to obtain S_{r+1} at every node x_i and at every time step t_r.

Once the values of microprestress and pore humidity are completely known, it is possible to tackle the structural problem of creep, shrinkage, and microcracking. The total strain $\epsilon(t)$ is expressed as (e.g. [36,37])

$$\epsilon(t)=\epsilon_{\mathrm{v}}+\epsilon_{\mathrm{f}}+\epsilon_{\mathrm{sh}}+\epsilon_{\mathrm{cr}}=\int_{t_0}^{t}\hat{J}(t,t')\sigma(x,\mathrm{d}t')+\epsilon_{\mathrm{sh}}+\epsilon_{\mathrm{cr}}. \tag{17}$$

Here t_0 is the instant of the set of concrete (i.e. at which concrete ceases to be a liquid); $\sigma(x, \mathrm{d}t')=[\partial\sigma(x, t')/\partial t']\mathrm{d}t'$ if σ varies continuously; $\hat{J}(t, t')=(1-\nu)J(t, t')$=biaxial compliance function of concrete in plane strain conditions, while $J(t, t')$ =uniaxial compliance function; and ν=Poisson ratio. The history integral is eliminated from Eq. (17) by approximating the compliance $C_g(\theta)$ in Eq. (6) by Dirichlet series [17];

$$C_g\approx A_0+\sum_{\mu=1}^{M}A_\mu\left[1-\exp\left(\frac{t-t'}{\tau_\mu}\right)\right]. \tag{18}$$

Parameters A_μ are age independent moduli approximating a continuous retardation spectrum [38]. Retardation times $\tau_\mu=10^{-3}, 10^{-2},\ldots, 10^{6}$ days, which are increased in a geometric progression ($\mu=1, 2,\ldots, M$), are chosen to represent the short-term as well as long-term behavior of the tower. The approximation in Eq. (18) leads to an equivalent age-independent Kelvin chain spring-dashpot model whose behavior is characterized by a fixed number of variables. This is a great advantage from the computational point of view because the stress history is replaced by the current stress values at the end of the last time step Δt, and thus need not to be stored. For the purpose of numerical analysis, Eq. (17) is written in an incremental form;

$$\Delta\epsilon=\Delta\epsilon_{\mathrm{v}}+\Delta\epsilon_{\mathrm{f}}+\Delta\epsilon_{\mathrm{sh}}+\Delta\epsilon_{\mathrm{cr}}. \tag{19}$$

To attain good accuracy with long time steps, one must use the so-called exponential algorithm [19,39]. In this algorithm the differential equations of creep are integrated analytically within each time step under the assumption that all the time dependent parameters are constant within the time step while changing only by jumps between the steps. Thus it was shown that the viscous strain increment $\Delta\epsilon_{\mathrm{v}}=\epsilon_{\mathrm{v},r+1}-\epsilon_{\mathrm{v},r}$, which depends on the stress increment $\Delta\sigma=\sigma_{r+1}-\sigma_r$, can be written as

$$\Delta\epsilon_{\mathrm{v}}=C_v\Delta\sigma+\Delta\epsilon_{\mathrm{v}}'' \tag{20}$$

where

$$C_v=q_1+\frac{1}{v_{r+1/2}}\left[A_0+\sum_{\mu=1}^{M}A_\mu(1-\lambda_\mu)\right] \tag{21}$$

$$\Delta\epsilon_{\mathrm{v}}''=\frac{1}{v_{r+1/2}}\sum_{\mu=1}^{M}(1-k_\mu)(A_\mu\sigma_r-\gamma_{\mu,r}) \tag{22}$$

and $\Delta y_\mu=\Delta t/\tau_\mu$, $k_\mu=\exp(-\Delta y_\mu)$, $\lambda_\mu=(1-k_\mu)/\Delta y_\mu$. Solidification (Eq. (4)) is introduced by means of the factor

$$\frac{1}{v_{r+1/2}}=\left(\frac{\lambda_0}{t_{r+1/2}}\right)^m+\frac{q_3}{q_2} \tag{23}$$

computed at time $t_{r+1/2}=t_r+\Delta t/2$. The flow strain increment,

$$\Delta\epsilon_{\mathrm{f}}=q_4'S(t_{r+1/2})\Delta S\hat{\sigma}_{r+1/2} \tag{24}$$

depends on microprestress $S(t_{r+1/2})$ and on the unknown stress $\hat{\sigma}_{r+1/2}=\sigma_r+\Delta\sigma/2$. The exponential algorithm can also be applied to the increment of cracking strain defined in Eq. (15), which gives [19]

$$\Delta\epsilon_{\mathrm{cr}}=\frac{1}{E_{\mathrm{cr}}}\Delta\sigma-\frac{\dot{E}_{\mathrm{cr}}}{E_{\mathrm{cr}}}\epsilon_{\mathrm{cr}}=C_{\mathrm{cr}}\Delta\sigma+\Delta\epsilon_{\mathrm{cr}}'' \tag{25}$$

$$\frac{1}{C_{\rm cr}} = \frac{1-\exp(-\Delta z)}{\Delta z} E_{\rm cr} \tag{26}$$

$$\Delta\epsilon''_{\rm cr} = [1-\exp(-\Delta z)] C_{\rm cr} \hat{\sigma}_{r+1} \tag{27}$$

where $C_{\rm cr}$=effective cracking compliance, $\Delta\epsilon_{\rm cr}''$=effective inelastic strain increment due to cracking, and $\Delta z = -\dot{E}_{\rm cr}\Delta\epsilon_{\rm cr}/E_{\rm cr}$. Finally, according to Eq. (11), the incremental shrinkage strain in Eq. (19) is written as $\Delta\epsilon_{\rm sh}=k_{\rm sh}\Delta h$. Eq. (19) may now be rewritten for every node $i=1,\ldots, n$ in the quasielastic form

$$\Delta\epsilon_i = (C_{v,i} + C_{{\rm cr},i})\Delta\sigma_i + \Delta\epsilon''_{{\rm v},i} + \Delta\epsilon_{\rm f} + \Delta\epsilon_{{\rm sh},i} + \Delta\epsilon''_{{\rm cr},i} \tag{28}$$

Because the wall is tall and symmetric, total strain ϵ may be considered to be uniform throughout the width, D. Assuming plane strain conditions, we may then analyze a slice of the wall having a unit thickness b. Vertical equilibrium in the horizontal cross section of the wall requires that

$$\int_0^D \sigma(x,t) b\,{\rm d}x = N(t) \tag{29}$$

or, in discrete incremental form,

$$\sum_{i=1}^{n} c_i \Delta\sigma_i \Delta x_i b = \Delta N_r \qquad (r = 1, 2, \ldots N) \tag{30}$$

where $\Delta\sigma_{i,r}=\sigma_{i,r+1}-\sigma_{i,r}$=increment of stress at node i; c_i=coefficients of trapezoidal numerical integration formula ($c_1=c_n=1/2$, $c_2=\ldots=c_{n-1}=1$); b=thickness of the wall; and $\Delta N_r=N(t_r+1)-N(t_r)$ increment of vertical load, which varies in time.

The step-by-step solution of stresses and strains in a generic time step Δt may proceed according to the following algorithm.

1. Evaluate $\Delta\epsilon_{{\rm sh},i}=k_{\rm sh}\Delta h_i$ ($i=1,\ldots, n$).
2. Evaluate $C_{v,i}$ and $\Delta\epsilon''_{{\rm v},i}$($i=1,\ldots, n$) from Eqs. (21) and (22).
3. Begin loop $I=1, 2,\ldots, N_{it}$.
4. From Eqs. (25), (26), and (27), evaluate $C_{{\rm cr},i}$ and $\Delta\epsilon''_{{\rm cr},i}$ ($i=1,\ldots n$) considering loading or unloading, and trial values of stresses and strains.
5. According to equilibrium condition (Eq. (30)), calculate:

$$\Delta\epsilon = \frac{\Sigma_{i=1}^{n} \frac{c_i\Delta x_i b}{C_{v,i}+C_{{\rm cr},i}} (\Delta\epsilon''_{{\rm v},i} + \Delta\epsilon_{\rm f} + \Delta\epsilon_{{\rm sh},i} + \Delta\epsilon''_{{\rm cr},i}) + \Delta N_r}{\Sigma_{i=1}^{n} \frac{c_i\Delta x_i b}{C_{v,i}+C_{{\rm cr},i}}} \tag{31}$$

6. From Eq. (28) calculate stress increment ($i=1, 2,\ldots, n$):

$$\Delta\sigma_i = \frac{\Delta\epsilon - \Delta\epsilon''_{{\rm v},i} - \Delta\epsilon_{\rm f} - \Delta\epsilon_{{\rm sh},i} - \Delta\epsilon''_{{\rm cr},i}}{C_{v,i} + C_{{\rm cr},i}} \tag{32}$$

7. Evaluate trial values of stresses and strains:

$$\hat{\sigma}_{i,r+1/2} = \sigma_{i,r} + \Delta\sigma_i/2 \tag{33a}$$

$$\hat{\epsilon}_{i,r+1/2} = \epsilon_{i,r} + \Delta\epsilon_i/2 \qquad (i = 1, 2, \ldots, n) \tag{33b}$$

8. Check the convergence criterion. If not met, go to 3.
9. End loop. Update stresses and strains ($i=1, 2,\ldots, n$):

$$\sigma_{i,r+1} = \sigma_{i,r} + \Delta\sigma_i \tag{34a}$$

$$\epsilon_{i,r+1} = \epsilon_{i,r} + \Delta\epsilon_i \tag{34b}$$

$$\gamma_{\mu,r+1} = \gamma_{\mu,r}k_\mu + \sigma_r A_\mu(1-k_\mu) + A_\mu(1-\lambda_\mu)\Delta\sigma_i \tag{34c}$$

10. Go to 1 and start the next time step Δt.

References

[1] G.M. Calvi, M.J.N. Priestley, Post collapse analyses of a medieval masonry tower, in: D. Abrams (Ed.), 5th North American Masonry Conference, Univ. of Illinois, Urbana–Champaign, Illinois, 1990, pp. 713–722.

[2] L. Binda, G. Gatti, G. Mangano, C. Poggi, G. Sacchi Landriani, The collapse of the Civic Tower of Pavia: a survey of the materials and structure, Mason. Int. 6 (1) (1992) 11–20.

[3] A. Anzani, L. Binda, G. Mirabella Roberti, The effect of heavy persistent actions into the behaviour of ancient masonry, Mat. Struct., RILEM 33 (228) (2000) 251–261.

[4] D. Ferretti, Z.P. Bažant, Stability of ancient masonry towers: moisture diffusion, Cem. Concr. Res. 36 (7) (2006) 1379–1388.

[5] G.M. Calvi, Mechanical Tests on the Masonry of the Civic Tower of Pavia, Joint Research between University of Pavia and Italian Ministry of Public Works, University of Pavia, 1990 (in Italian).

[6] A. Anzani, L. Binda, G. Melchiorri, Time dependent damage of rubble masonry walls, in: H. West (Ed.), 4th International Masonry Conference, British Masonry Society, London, 1995, pp. 341–351.

[7] D.R. Moorehead, Cementation by the carbonation of hydrated lime, Cem. Concr. Res. 16 (1986) 700–708.

[8] L. Brieger, F.H. Wittman, Numerical simulation of carbonation of concrete, in: F. Wittmann (Ed.), Material and Science Restoration, Tech. Akad. Esslingen, Ostfildern, 1986, pp. 635–640.

[9] A.V. Saetta, B.A. Schrefler, R. Vitaliani, The carbonation of concrete and the mechanism of moisture, heat and carbon dioxide flow through porous materials, Cem. Concr. Res. 23 (4) (1993) 761–772.

[10] A.V. Saetta, R. Vitaliani, Experimental investigation and numerical modeling of carbonation process in reinforced concrete structures: Part I. Theoretical formulation, Cem. Concr. Res. 34 (4) (2004) 571–579.

[11] L.B. Sickels Taves, Creep, shrinkage and mortars in historic preservation, J. Test. Eval. 23 (1995) 447–452.

[12] N.G. Shrive, E. Sayed-Ahmed, D. Tilleman, Creep analysis of clay masonry assemblages, Can. J. Civ. Eng. 24 (3) (1997) 367–379.

[13] G. Baronio, L. Binda, N. Lombardini, The role of brick pebbles and dust in conglomerates based on hydrated lime and crushed bricks, Constr. Build. Mater. 11 (1) (1997) 33–34.

[14] Z.P. Bažant, Criteria for rational prediction of creep and shrinkage of concrete, Rev. Française Génie Civil 3 (3/4) (1999) 61–89.

[15] Z.P. Bažant, S. Baweja, Creep and shrinkage prediction model for analysis and design of concrete structures: model B3, in: A. Al-Manaseer (Ed.), Adam Neville Symposium: Creep and Shrinkage–Structural Design Effects, ACI SP-194, Am. Concrete Institute, Farmington Hills, Michigan, 2000, pp. 1–83.

[16] Z.P. Bažant, A.B. Hauggaard, S. Baweja, F.J. Ulm, Microprestress-solidification theory for concrete creep: I. Aging and drying effects, J. Eng. Mech., ASCE 123 (11) (1997) 1188–1194.

[17] Z.P. Bažant, A.B. Hauggaard, S. Baweja, Microprestress-solidification theory for concrete creep: II. Algorithm and verification, J. Eng. Mech., ASCE 123 (11) (1997) 1195–1201.

[18] E.G. Swenson, P.J. Sereda, Some ageing characteristics of lime, J. Appl. Chem. 17 (1967) 198–202.

[19] Z.P. Bažant, J.C. Chern, Strain softening with creep and exponential algorithm, J. Eng. Mech., ASCE 111 (3) (1985) 391–415.

[20] Z.P. Bažant, Y. Xi, Drying creep of concrete: constitutive model and new experiments separating its mechanisms, Mat. Struct., RILEM 27 (165) (1994) 3–14.

[21] Z.P. Bazant, S. Baweja, in collaboration with RILEM Committee TC 107-GCS, Creep and shrinkage prediction model for analysis and design of concrete structures—model B3, Mat. Struct., RILEM 28 (180) (1995) 357–365.
[22] J.J. Brooks, Composite modelling of masonry deformation, Mat. Struct., RILEM 23 (1990) 241–251.
[23] J. Lanas, J.I. Alvarez, Masonry repair lime-based mortars: factors affecting the mechanical behavior, Cem. Concr. Res. 33 (2003) 1867–1876.
[24] E.G. Swenson, P.J. Sereda, Mechanism of the carbonation shrinkage of lime and hydrated lime, J. Appl. Chem. 18 (1968) 111–117.
[25] J. Planas, M. Elices, Drying shrinkage effects on the modulus of rupture, in: Z.P. Bažant, I. Carol (Eds.), 5th Int. RILEM Symp., Barcelona, RILEM, E & FN Spon, London, 1993, pp. 357–368.
[26] Z.P. Bažant, B.H. Oh, Crack band theory for fracture of concrete, Mat. Struct., RILEM 16 (93) (1983) 155–177.
[27] Z.P. Bažant, H. Ohtsubo, Stability conditions for propagation of a system of cracks in a brittle solid, Mech. Res. Commun. 4 (5) (1977) 353–366.
[28] Z.P. Bažant, L. Cedolin, Stability of Structures: Elastic, Inelastic, Fracture and Damage Theories, Oxford University Press, New York, 1991.
[29] Z.P. Bažant, W.J. Raftshol, Effect of cracking in drying and shrinkage specimens, Cem. Concr. Res. 12 (2) (1982) 209–226 (disc. 797–798.).
[30] CEB-FIP, CEB-FIP model code 1990, Thomas Telford, Lausanne, 1992.
[31] J.P.A.G. van Zijl, R. de Borst, J.G. Rots, The role of crack dependence in the long-term behaviour of cementitious materials, Int. J. Solids Struct. 38 (2001) 5063–5079.
[32] D. Lenczer, In-situ measurement of creep movement in a brick masonry tower block, Mason. Int. 8 (1) (1986) 17–20.
[33] C. Groot, J. Larbi, The influence of water flow (reversal) on bond strength development in young masonry, Heron 44 (2) (1999) 63–78.
[34] E. Papa, A. Taliercio, L. Binda, Safety assessment of ancient masonry towers, in: B.H.V. Topping, C.A. Mota Soares (Eds.), 2nd Int. Congr. Studies in Ancient Structures, vol. 1, Istanbul, Turkey, 2001, pp. 345–354.
[35] L.F. Shampine, Numerical Solution of Ordinary Differential Equations, Chapman & Hall, New York, 1994.
[36] Z.P. Bažant, Mathematical models for creep and shrinkage of concrete, in: Z.P. Bažant, F. Wittmann (Eds.), Creep and Shrinkage of Structures, John Wiley, London, 1982, pp. 163–256.
[37] RILEM, State of the art in mathematical modeling of creep and shrinkage of concrete, in: C. Committee TC 69, Z.P. Bažant (Eds.), Mathematical Modeling of Creep and Shrinkage of Concrete, RILEM, J. Wiley, Chichester and New York, 1988, pp. 57–215.
[38] Z.P. Bažant, Y. Xi, Continuous retardation spectrum for solidification theory of concrete creep, J. Eng. Mech., ASCE 121 (2) (1995) 281–288.
[39] Z.P. Bažant, Numerical solution of nonlinear creep problems with application to plates, Int. J. Solids Struct. 7 (1971) 83–97.